IOP Publishing Phys. Med. Biol. 63 (2018) 085012 (15pp) https://doi.org/10.1088/1361-6560/aab957

Physics in Medicine & Biology

IPEM Institute of Physics and Engineering in Medicine

RECEIVED
11 January 2018

REVISED
2 March 2018

ACCEPTED FOR PUBLICATION
23 March 2018

PUBLISHED
19 April 2018

PAPER

Motion induced interplay effects for VMAT radiotherapy

Anneli Edvardsson[1,5], **Fredrik Nordström**[2,3], **Crister Ceberg**[1] and **Sofie Ceberg**[1,4]

[1] Department of Medical Radiation Physics,Clinical Sciences, Lund University, Lund, Sweden
[2] Department of Medical Physics and Biomedical Engineering, Sahlgrenska University Hospital, Gothenburg, Sweden
[3] Department of Radiation Physics, Institute of Clinical Sciences, Sahlgrenska Academy at University of Gothenburg, Gothenburg, Sweden
[4] Department of Hematology, Oncology and Radiation Physics, Skåne University Hospital, Lund, Sweden
[5] Author to whom any correspondence should be addressed.

E-mail: anneli.edvardsson@med.lu.se

Keywords: interplay effects, breathing motion, intrafractional motion, VMAT, RapidArc, radiotherapy

Abstract

The purpose of this study was to develop a method to simulate breathing motion induced interplay effects for volumetric modulated arc therapy (VMAT), to verify the proposed method with measurements, and to use the method to investigate how interplay effects vary with different patient- and machine specific parameters.

VMAT treatment plans were created on a virtual phantom in a treatment planning system (TPS). Interplay effects were simulated by dividing each plan into smaller sub-arcs using an in-house developed software and shifting the isocenter for each sub-arc to simulate a $\sin^6$ breathing motion in the superior–inferior direction. The simulations were performed for both flattening-filter (FF) and flattening-filter free (FFF) plans and for different breathing amplitudes, period times, initial breathing phases, dose levels, plan complexities, CTV sizes, and collimator angles. The resulting sub-arcs were calculated in the TPS, generating a dose distribution including the effects of motion. The interplay effects were separated from dose blurring and the relative dose differences to 2% and 98% of the CTV volume ($\Delta D_{98\%}$ and $\Delta D_{2\%}$) were calculated. To verify the simulation method, measurements were carried out, both static and during motion, using a quasi-3D phantom and a motion platform.

The results of the verification measurements during motion were comparable to the results of the static measurements. Considerable interplay effects were observed for individual fractions, with the minimum $\Delta D_{98\%}$ and maximum $\Delta D_{2\%}$ being −16.7% and 16.2%, respectively. The extent of interplay effects was larger for FFF compared to FF and generally increased for higher breathing amplitudes, larger period times, lower dose levels, and more complex treatment plans. Also, the interplay effects varied considerably with the initial breathing phase, and larger variations were observed for smaller CTV sizes.

In conclusion, a method to simulate motion induced interplay effects was developed and verified with measurements, which allowed for a large number of treatment scenarios to be investigated. The simulations showed large interplay effects for individual fractions and that the extent of interplay effects varied with the breathing pattern, FFF/FF, dose level, CTV size, collimator angle, and the complexity of the treatment plan.

1. Introduction

In recent years several new radiotherapy techniques have been developed that enable a more conform dose distribution, such as intensity modulated radiotherapy (IMRT), volumetric modulated arc therapy (VMAT) and intensity modulated proton therapy (IMPT). One disadvantage of these novel treatment techniques, however, is their increased sensitivity to motion (Bortfeld *et al* 2004). Respiration is one of the dominating motions affecting the radiotherapy treatment, primarily in the thorax and upper abdomen, which might cause deviations between

the planned and delivered dose distributions in the form of dose blurring and interplay effects (Bortfeld *et al* 2004). Dose blurring occurs regardless of the treatment technique and results in decreased dose at the edges of the target volume and increased dose to nearby organs at risk (OAR). Interplay effects, however, occur only for dynamic treatment techniques such as IMRT, VMAT and IMPT, where there is a simultaneous movement of machine parts (for example the multileaf collimators (MLC)) and the target volume, resulting in hotspots and coldspots in the dose distribution. Dose blurring can be described as a convolution of the dose distribution with the motion pattern and can be managed with increased margins. However, increased margins are not sufficient to adequately account for the interplay effects. Different approaches to quantify interplay effects for IMRT and VMAT have been proposed, including statistical analysis (Bortfeld *et al* 2002), simulations (Court *et al* 2008, Poulsen *et al* 2012), and measurements (Jiang *et al* 2003, Duan *et al* 2006, Court *et al* 2008, 2010, Ong *et al* 2011, 2013, Rao *et al* 2012, Ceberg *et al* 2013). Using these different methods, it has been shown that extensive interplay effects may occur and that the extent depends on patient- and machine specific parameters, such as breathing pattern (Court *et al* 2008, 2010, Ong *et al* 2011, 2013), dose level (Rao *et al* 2012), dose rate (Jiang *et al* 2003, Court *et al* 2008, Ong *et al* 2013), collimator angle (Court *et al* 2008), and the complexity of the treatment plan (Court *et al* 2010, Ong *et al* 2011).

Although it has been shown that the dosimetric effects of interplay average out for multiple fractions (Bortfeld *et al* 2002, 2004, Jiang *et al* 2003, Duan *et al* 2006, Court *et al* 2010, Rao *et al* 2012, Ong *et al* 2013), we believe it is also of interest to investigate the dosimetric effect of interplay for individual fractions. In radiotherapy of today, we generally seek to deliver a homogeneous dose distribution to the tumour at each fraction, and the biological consequences of not fulfilling this aim are still not well known. Moreover, we are moving more towards hypofractionated radiotherapy (Jagsi *et al* 2014, Stokes *et al* 2017), where the treatment is delivered in few fractions, and then the averaging effect is not as pronounced. Much has been done but a comprehensive investigation of all relevant parameters is still lacking. Here we apply novel evaluation tools to define and evaluate interplay effects.

The aim of this study was to develop a tool to simulate motion induced interplay effects for the VMAT technique RapidArc (Varian Medical Systems, Palo Alto, CA, USA) using the commercially available treatment planning system (TPS) Eclipse (version 13.6) and to verify this tool with dosimetric measurements. This tool then allowed for a systematic investigation of how the extent of interplay effects depend on a large set of different parameters, such as breathing amplitude, period time, initial breathing phase, dose level, FF/FFF, collimator angle, CTV size, and the complexity of the treatment plan, to be performed. Also, the effect of multiple fractions was investigated. To our knowledge, an equally comprehensive investigation of the dependence of interplay effects has previously not been reported in a single study for RapidArc treatment.

2. Material and methods

RapidArc treatment plans were created on a virtual phantom of the Delta4 (ScandiDos, Uppsala, Sweden) in the Eclipse TPS (Version 13.6, Varian Medical Systems, Palo Alto, CA, USA), with the diameter and length of 22 cm and 40 cm, respectively. Interplay effects were then simulated for different breathing patterns for each treatment plan through dividing the plans into smaller sub-arcs and shifting the isocenter for each sub-arc. To verify the simulation method, five treatment plans were measured during motion, using the Delta4 phantom and the HexaMotion platform (ScandiDos, Uppsala, Sweden). The virtual phantom, treatment plans, simulation method and verification measurements are described in more detail below.

2.1. Virtual phantom

All simulations were performed in the Eclipse TPS on a virtual phantom of the cylindrically shaped Delta4 phantom with the diameter and length of 22 and 40 cm, respectively, and a mass density of 1.152 g cm^{-3} (figure 1). The virtual phantom contained artificial structures in the form of a spherical CTV and two cylindrical OARs (Ø 2 and 4 cm). The diameter of the CTV was 1, 3, 5 or 8 cm and the corresponding volumes were 0.5, 14, 65 and 268 cm^3. The CTV was centrally positioned in the phantom and the two OARs were situated 90° relative to each other towards the edge of the phantom, with a minimal distance between the surface of the CTV and OARs of 1.0 and 1.5 cm, respectively (figure 1). To account for the dose blurring effect in the edges of the target volume, ITVs were created by adding a margin to the CTV in the direction of motion (superior–inferior (S–I) direction) corresponding to each simulated breathing amplitude (section 2.3). Finally, PTVs were generated by applying an additional isotropic margin of 5 mm to the ITV.

2.2. Treatment plans

A TrueBeam linear accelerator with Millenium MLC (Varian Medical Systems, Palo Alto, CA, USA) was used for the treatment planning and delivery of the plans. Single coplanar arc 6 MV RapidArc plans with 358° counterclockwise rotation and 178 control points were created in the Eclipse TPS. The dose was calculated using the anisotropic analytic algorithm (AAA, version 13.6.23) with a calculation grid of 1 mm for the CTV diameter

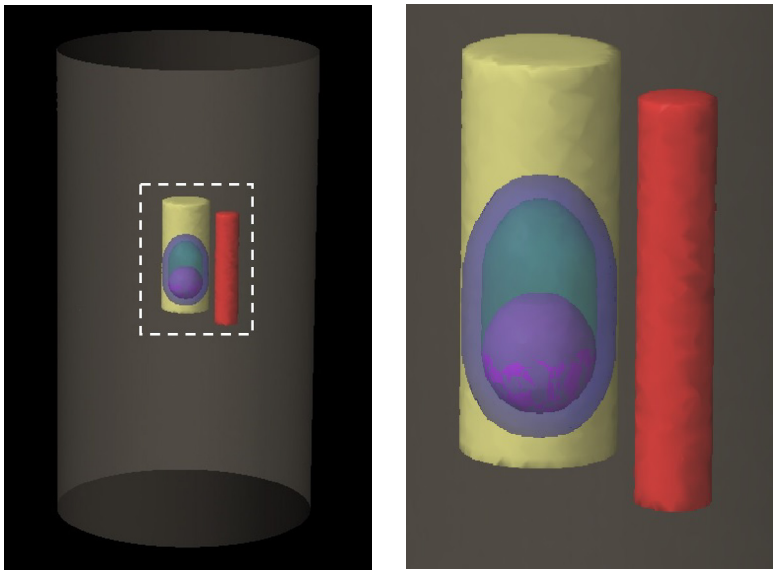

(a) (b)

Figure 1. A 3D view of the virtual phantom, containing a CTV (purple), ITV (green), PTV (blue) and two organs at risk (red and yellow), for the CTV diameter 3 cm and breathing amplitude 20 mm. A magnification of the white dashed box in (a) is displayed in (b).

1 cm and 2.5 mm for the CTV diameters 3, 5 and 8 cm. During optimization, constraints were set on the PTV and OARs together with a normal tissue objective, to receive a uniform dose to the PTV (highest priority) and at the same time keep the doses to the OARs as low as possible (lower priority). The dose was prescribed for one fraction and normalized to the mean dose of the PTV.

Both FF and FFF plans were created and the CTV size, dose level, collimator angle and the complexity of the treatment plan was varied. One default plan was first generated and the parameters were then changed one at a time, resulting in a total of 17 different treatment plans (table 1). The CTV diameter was either 1, 3, 5 or 8 cm, the dose level was 2, 5, 10 or 15 Gy and the collimator angle was 0, 30, 45 or 90°. The maximum dose rate was 600 and 1400 MU min^{-1} for FF and FFF, respectively. Four different levels of plan complexity were generated (C_1, C_2, C_3 and C_4) by changing the MU/Gy constraint and priorities of the OAR constraints in the optimizer while the prescribed dose was kept constant, with the assumption that a higher MU/Gy results in more MLC movement and smaller field openings and hence more complex treatment plans. The number of MU/Gy and beam-on times for the different treatment plans are presented in table 1.

2.3. Respiratory motion

To simulate respiratory motion in the S–I direction, an asymmetric sinusoid model was used which implies that more time is spent in the exhale phase than in the inhale phase (figure 4) (Lujan *et al* 1999, Seppenwoolde *et al* 2002). The motion was then given by

$$A = A_0 \sin^6\left(\frac{\pi t}{T} + \varphi\right) \tag{1}$$

where t is the time, A_0 the breathing amplitude, T the period time and φ the initial breathing phase. All possible combinations of six breathing amplitudes (5, 10, 15, 20, 25 and 30 mm, peak-to-peak), three period times (3, 5 and 7 s) and four initial breathing phases (0, $\frac{\pi}{2}$, π and $\frac{3\pi}{2}$) were simulated, chosen to be representative of real patient respiratory motion (Seppenwoolde *et al* 2002), giving a total of 72 breathing patterns. The initial breathing phases are further referred to as percentages, where 0, 25, 50 and 75% correspond to the phase angles 0, $\frac{\pi}{2}$, π, and $\frac{3\pi}{2}$, respectively.

2.4. Simulation method

The simulation method is based on rigid motion and include five steps, which are illustrated in figure 2 and further explained in sections 2.4.1–2.4.3. To investigate how interplay effects depend on the breathing pattern, simulations were performed for all 72 breathing patterns (section 2.3) using the default treatment plan (table 1). Also, simulations were performed for all treatment plans in table 1 to investigate how interplay effects vary with different patient- and machine specific parameters. Then, a breathing amplitude of 20 mm and a period time of 7 s were used and all four initial breathing phases (0, 25, 50 and 75%) were simulated. In total, 136 simulations

Table 1. The different combinations of CTV diameter, dose level, filter (FF: flattening filter, FFF: flattening-filter free), collimator angle and complexity level (C_1, C_2, C_3 and C_4) for the treatment plans used for the simulations as well as the number of MU/Gy and beam-on times.

Plan nr	CTV Ø (cm)	Dose level (Gy)	FF/FFF	Collimator angle (°)	Complexity level	MU/Gy	Beam-on time (min)
1[a]	3	2	FFF	30	C_3	349.9	1.00
2	3	2	FFF	30	C_1	222.6	1.00
3	3	2	FFF	30	C_2	284.7	1.00
4	3	2	FFF	30	C_4	432.0	1.00
5	3	2	FFF	0	C_3	332.1	1.00
6	3	2	FFF	45	C_3	329.3	1.00
7	3	2	FFF	90	C_3	361.0	1.00
8	1	2	FFF	30	C_3	349.0	1.00
9	5	2	FFF	30	C_3	351.7	1.00
10	8	2	FFF	30	C_3	351.0	1.00
11	3	5	FFF	30	C_3	349.9	1.25
12	3	10	FFF	30	C_3	349.9	2.50
13	3	15	FFF	30	C_3	349.9	3.75
14	3	2	FF	30	C_3	309.6	1.06
15	3	5	FF	30	C_3	309.6	2.58
16	3	10	FF	30	C_3	309.6	5.16
17	3	15	FF	30	C_3	309.6	7.74

[a] Default plan.

were carried out. An in-house developed program, written in Visual C# (Microsoft Corporation, Redmond, WA, USA), was used to divide the RapidArc treatment plans into sub-arcs (Nordström 2012, Nordström *et al* 2013). The calculations of control points for each bin, the isocenter shifts, and the convolution of the static dose distributions were performed in Matlab (R2014b, Mathworks, Natick, MA, USA). The final dosimetric analysis was carried out using the Medical Interactive Creative Environment (MICE), version 0.4.0.94 (available at www.gentleradiotherapy.se) (Nyholm *et al* 2015).

2.4.1. *Calculation of control points for each bin*

In a RapidArc treatment, the radiation is delivered as the gantry rotates around the patient while the position of the MLC, gantry speed, and dose rate vary continuously (Otto 2008). The cumulative number of MUs, gantry angle, and MLC positions are specified in discrete, so called control points at a fixed angular interval. Linearity is assumed between the control points.

For the delivery of a RapidArc plan, the maximum gantry rotation speed is used if possible and the number of MUs delivered for each control point is determined by varying the dose rate. If a larger number of MUs is to be delivered for each control point, the gantry rotation speed is slowed down and the maximum dose rate is used. Based on this information, the maximum number of MUs that can be delivered without decreasing the gantry rotation speed can be calculated, which is further described by Park *et al* (2014). If the number of MUs is lower than this maximum value, the time between the control points can be calculated as the ratio of the angular interval and the maximum gantry rotation speed. If the number of MUs is higher than this maximum value, however, the time between the control points can be calculated as the ratio of the number of MUs delivered between the control points and the maximum dose rate.

In this way, the time intervals for the control points of the original treatment plans were generated. Time intervals corresponding to 1 mm position bins generated from the breathing pattern (section 2.3) were calculated, and the corresponding control points for the bins could then be obtained through linear interpolation.

2.4.2. *Division into sub-arcs*

The original DICOM-RT treatment plans were then divided into sub-arcs using the in-house developed software, where the number of sub-arcs equals the number of 1 mm bins. The original plan files were imported into this software and new beams were generated where each new beam corresponded to the part of the treatment delivered during the bin. Control points, corresponding to the machine parameters at the start and the end of each bin, were created through linear interpolation between control points of the original plan. Any control points in between the start and the end of the bin were propagated from the original plan unaltered. Fixed plan parameters, such as the jaw positions and the collimator angle, were only transferred from the original plan to the first control point of each beam of the modified plan, i.e. the plan consisting of sub-arcs. The time varying parameters (fraction of MUs, gantry angle and MLC positions) for the new beams were propagated to the corresponding control points

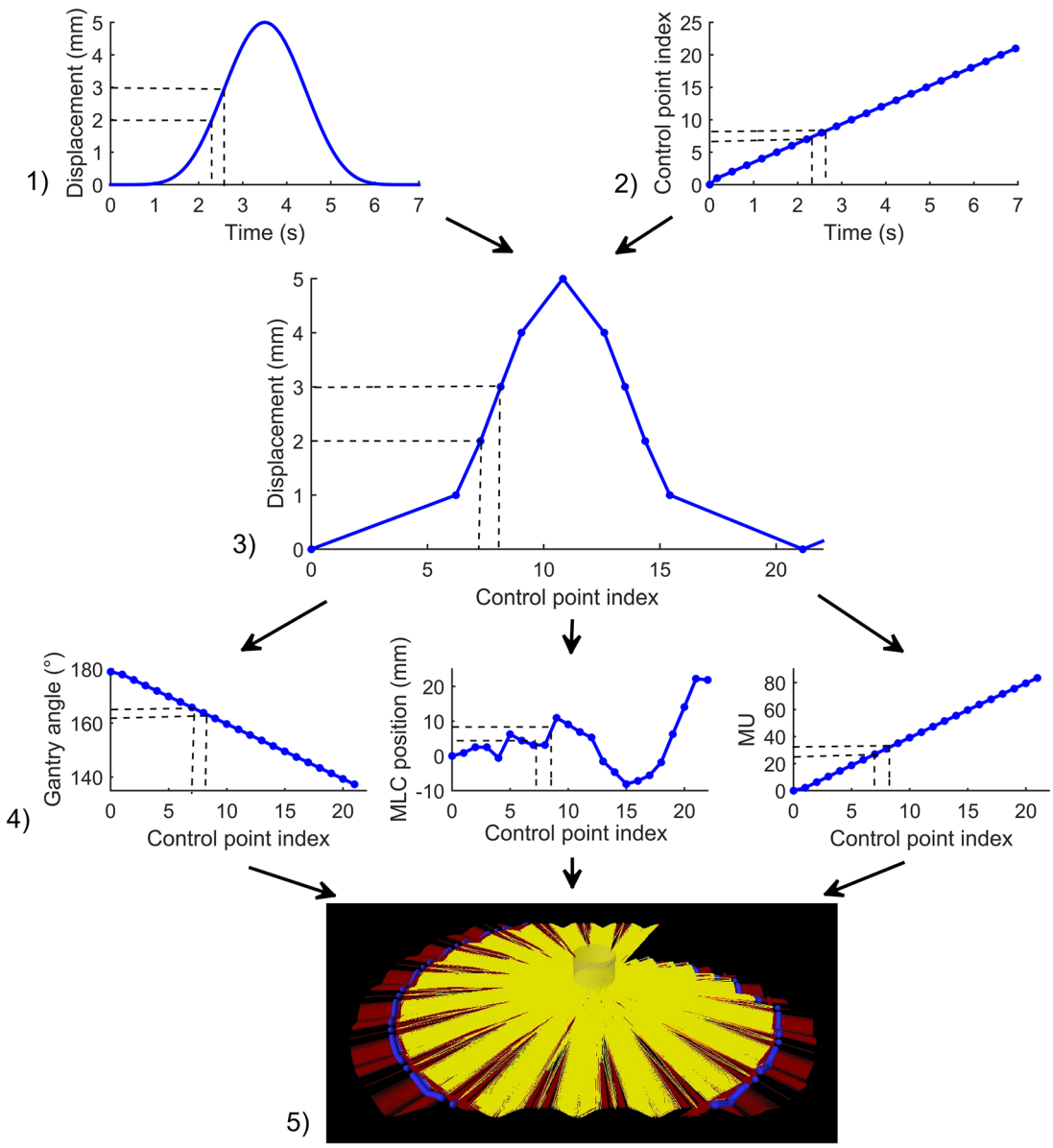

Figure 2. Schematic illustration of the simulation method. Time intervals corresponding to 1 mm position bins were generated from the breathing pattern (1) and the time for each control point was determined from the treatment plan (2). The control points for the 1 mm bin were then obtained through linear interpolation (3). The number of MUs, the MLC position, and the gantry angle were obtained for each generated control point, creating a sub-arc corresponding to the treatment delivered during the position bin (4). The isocenter was shifted for each sub-arc according to the breathing pattern and the resulting treatment plan was calculated in the TPS (5).

of the modified plan. Since the Eclipse TPS requires three control points to calculate dose and if the number of created control points according to above were two, an additional control point was inserted equidistant between the existing control points through linear interpolation. In this way all generated beams always contained at least three control points. Since the fraction of MUs (i.e. cumulative meterset weight) is always given in the range from 0 to the value of the final cumulative meterset weight (1 for VMAT plans from Eclipse) in the DICOM-RT plan file, these values were rescaled for the new control points and the total MUs (i.e. beam meterset) were adjusted accordingly.

2.4.3. Isocenter shifts

The isocenter of each sub-arc was then shifted in the S–I direction according to the breathing pattern (equation (1)), in the opposite direction of the motion, using an in-house developed Matlab script. The applied isocenter shifts corresponded to the average position within the 1 mm bins and was calculated as the integral of the breathing curve (equation (1)) divided by the time interval for each bin. The modified DICOM-RT plan file, including the isocenter shifts, was then imported into the Eclipse TPS, where the dose was calculated for each sub-arc, generating a simulated dose distribution including the effects of motion.

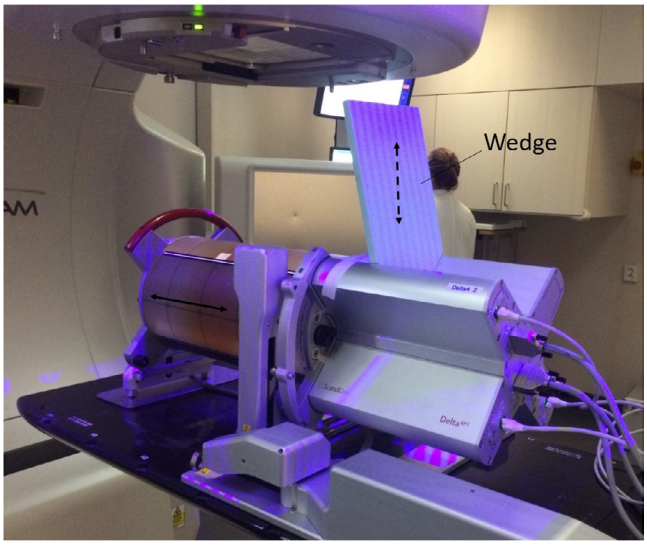

Figure 3. The setup of the Delta4 phantom and HexaMotion platform used for the verification measurements. A wedge was positioned on the Delta4 phantom to generate vertical motion (dashed arrow) registered by the gating function of the Catalyst system, since the HexaMotion was only moving in the superior–inferior direction (solid arrow).

Table 2. The different combinations of CTV diameter, dose level and complexity level for the treatment plans used for the verification measurements as well as the number of MU/Gy, beam-on times, amplitudes and the nominal/actual period times. All treatment plans were FF and had the collimator angle 30°.

Plan nr	CTV Ø (cm)	Dose level (Gy)	Complexity level	MU/Gy	Beam-on time (min)	Amplitude (mm)	Nominal/actual period time (s)
1	8	2	C_3	341.1	1.15	5	3.0/2.6
2	8	2	C_3	348.3	1.17	20	7.0/6.2
3	3	2	C_3	309.6	1.06	20	7.0/6.2
4	8	10	C_3	348.3	5.80	20	7.0/6.2
5	8	2	C_1	200.4	1.00	20	7.0/6.2

2.4.4. Dosimetric analysis

Due to the added ITV (as described in section 2.1), with a margin corresponding to each investigated breathing amplitude, the dosimetric effects of dose blurring at the edges of the target volume are not included in the analysis. However, respiratory motion also results in a blurring of any dose heterogeneities within the CTV. To account for this effect, and thus to separate interplay effects from all other dose blurring, the original static dose distribution was convolved with the motion pattern described in equation (1) (Bortfeld *et al* 2004, Ceberg *et al* 2013). This was achieved by shifting the dose distribution in 1 mm bins and weighting each dose distribution by the fraction of the total time spent in that bin. The convolved dose distribution was then obtained by summing all these dose distributions.

The convolved dose distribution was subtracted from the simulated dose distribution, and the residual dose differences could then be interpreted as solely due to interplay effects. The relative dose differences to 98% and 2% of the CTV volume ($\Delta D_{98\%}$ and $\Delta D_{2\%}$) were calculated, corresponding to the near minimum- and maximum dose differences. The analysis was performed on the CTV volume to quantify the dosimetric effects of only interplay and not including any dose blurring.

To investigate the effect of multiple fractions, the $\Delta D_{98\%}$ and $\Delta D_{2\%}$ for the difference between the average dose distribution for the four different initial breathing phases (0, 25, 50 and 75%) and the convolved dose distribution was calculated for all the scenarios investigated. This provides an estimate of the interplay effect on the total accumulated dose distribution for a four-fraction treatment, assuming rectangular probability distribution for the initial breathing phase.

2.5. Verification measurements

To verify the proposed simulation method, five different treatment plans were delivered to the Delta4 phantom positioned on the motion platform HexaMotion (figure 3), which was either static or moving in a $\sin^6$ motion trajectory in the S–I direction during irradiation. The measured treatment plans had different CTV diameters

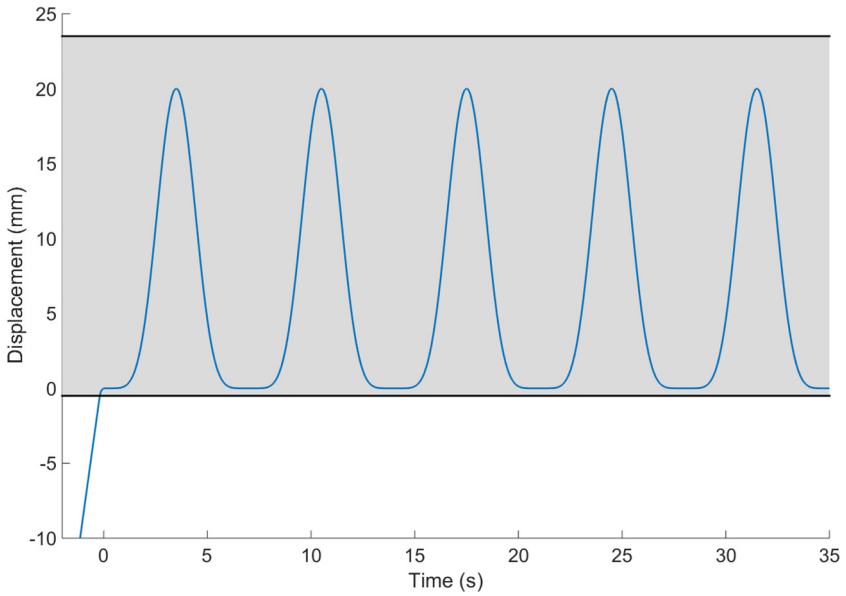

Figure 4. Example of a $\sin^6$ motion trajectory used for the verification measurements, with an amplitude of 20 mm and period time of 7 s. The irradiation was triggered when the motion trajectory (blue) entered the beam-on window (grey).

Table 3. Comparison of the measured dose distribution during motion (D_{meas}^{motion}) and the simulated dose distribution including effects of motion (D_{sim}^{motion}) as well as the static measured dose distribution (D_{meas}^{static}) and the original simulated dose distribution without motion (D_{sim}^{static}), presented as gamma pass rate for the criteria 3%/2 mm global dose with a cut-off dose of 15%.

	Gamma pass rate (%)	Gamma pass rate (%)
Plan nr	D_{meas}^{motion} versus D_{sim}^{motion}	D_{meas}^{static} versus D_{sim}^{static}
1	93.6	93.0
2	97.6	93.5
3	100.0	98.4
4	95.0	93.4
5	100.0	100.0
Median (range)	97.5 (93.6–100.0)	93.5 (93.0–100.0)

(3 and 8 cm), dose levels (2 and 10 Gy), and complexity level (C_1 and C_3) (table 2). All treatment plans were FF and the collimator angle was 30°. The measurements were performed for two different motion patterns, with amplitude and period time of 5 mm and 3 s, or 20 mm and 7 s, respectively. The nominal period times were set to 3 and 7 s. In reality, however, the HexaMotion period times were slightly shorter, 2.6 and 6.2 s, and these period times were also used in the comparative simulations. Hence, the same period times were used for both the measurements and the simulations.

The respiratory gating function of the optical surface scanning system Catalyst (C-rad Positioning AB, Uppsala, Sweden) was used to synchronize the motion and the treatment delivery, i.e. to trigger the irradiation in the desired breathing phase (0%). The HexaMotion platform was moving in the S–I direction during the measurements, thus in the same directions as for the simulations. However, only motion in the vertical direction was registered by the gating function of the Catalyst system. To generate vertical motion, a wedge was positioned on the rear end of the Delta4 phantom (figure 3). The Delta4 phantom was initially positioned outside the beam-on window and by a fast movement of the phantom into the beam-on window it was possible to trigger the radiation in the desired initial breathing phase (figure 4).

Simulated dose distributions including effects of motion (D_{sim}^{motion}) were calculated for the measured breathing patterns (20 mm/6.2 s/0% and 5 mm/2.6 s/0%) using the simulation method presented above. The measured dose distribution during motion (D_{meas}^{motion}) and the static measured dose distribution (D_{meas}^{static}) were compared to D_{sim}^{motion} and the original static simulated dose distribution (D_{sim}^{static}), respectively, using gamma analysis (Low *et al* 1998) in the Delta4 software. The criteria 3%/2 mm global dose and a cut-off dose of 15% were used. These

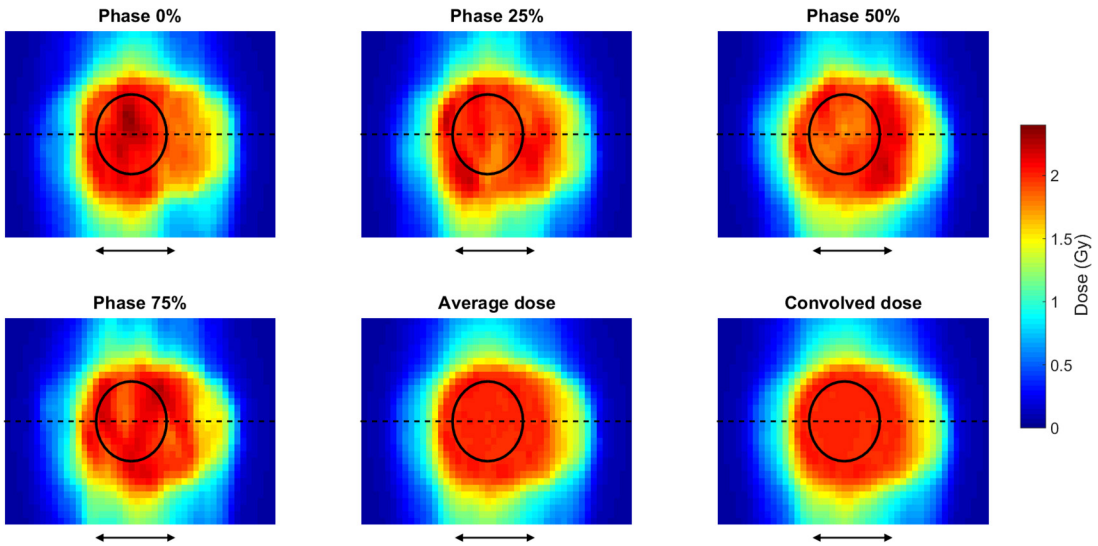

Figure 5. Examples of sagittal views of the simulated dose distribution for the four different initial breathing phases (0, 25, 50 and 75%), for the default treatment plan. In addition, the average dose distribution for the four initial breathing phases and the convolved dose distribution are displayed. The black circle correspond to the contour of the CTV volume. The arrows show the direction of the simulated motion.

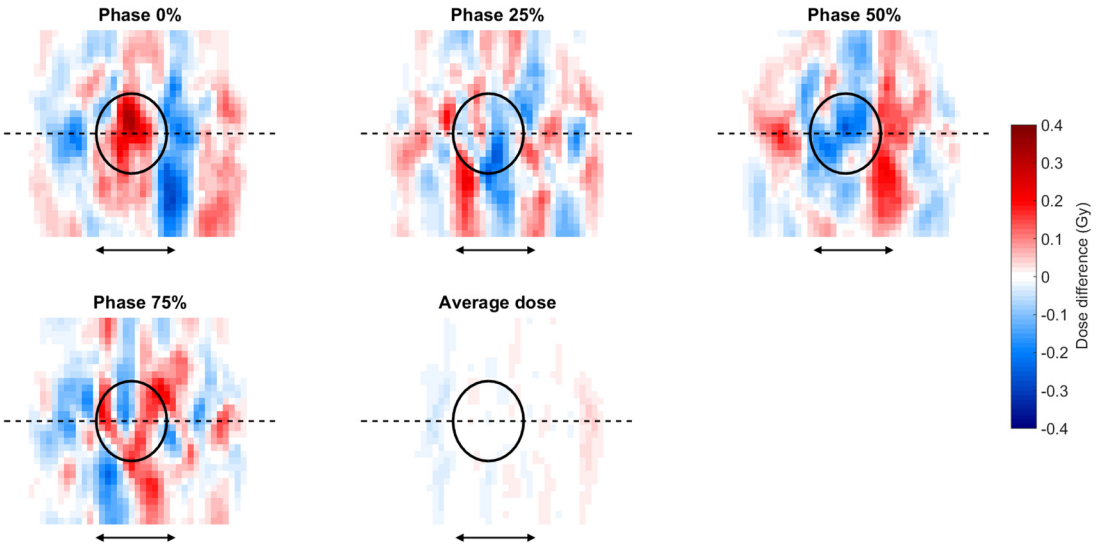

Figure 6. Examples of sagittal views of the difference between the simulated dose distributions for the four different initial breathing phases (0, 25, 50 and 75%) and the convolved dose distribution, for the default treatment plan. In addition, the difference between the average dose distribution for the four initial breathing phases and the convolved dose distribution is displayed. The black circle correspond to the contour of the CTV volume. The arrows show the direction of the simulated motion.

criteria were chosen since they are used clinically at our department and were found suitable with respect to the uncertainties in the dosimetric system used for the measurements.

3. Results

3.1. Verification measurements

The results of the verification measurements showed good agreement between D_{meas}^{motion} and D_{sim}^{motion} with a median gamma pass rate of 97.5%, comparable to the median gamma pass rate of D_{meas}^{static} and D_{sim}^{static} of 93.5% (table 3). Based on these results, we decided that the proposed simulation method could be used for further simulations.

3.2. Simulations

Examples of simulated dose distributions for the four different initial breathing phases, as well as the average dose distribution for the four phases, representing the effect of multiple fractions, are presented in figure 5,

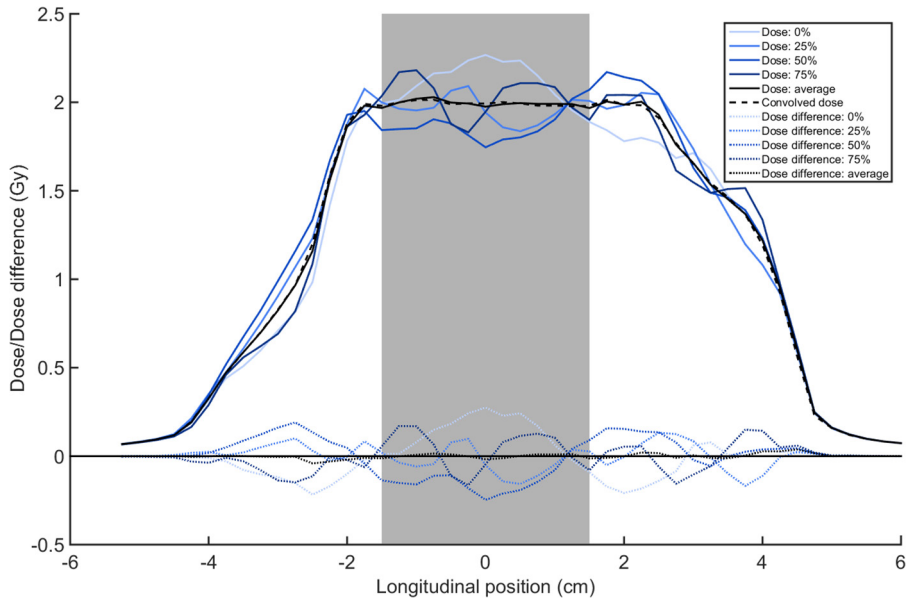

Figure 7. The solid lines represent dose profiles along the black dashed lines in figure 5 and the dotted lines represent profiles of the absolute dose differences along the black dashed lines in figure 6. The four different initial breathing phases (0, 25, 50 and 75%) are displayed in different shades of blue and the average of the four initial breathing phases in black. The convolved dose is displayed as a dashed black line for comparison. The grey area corresponds to the CTV volume.

together with the convolved dose distribution for comparison. The corresponding dose differences compared to the convolved dose distribution, i.e. interplay effects, are presented in figure 6 and profiles of the doses and dose differences (according to the black dashed lines in figures 5 and 6) are presented in figure 7. Substantial differences between the dose distributions for the different initial breathing phases and the convolved dose distribution were observed, indicating considerable dosimetric effects of interplay for a single fraction. The minimum $\Delta D_{98\%}$ and maximum $\Delta D_{2\%}$ observed for the CTV volume were −16.7% and 16.2% (figure 9), respectively, for the initial breathing phases 25 and 75%, and for the treatment plan with the highest complexity level (plan nr 4 in table 1). Hence, both under- and over-dosed volumes were observed within the CTV. Further, values of $\Delta D_{98\%}$ and $\Delta D_{2\%}$ in the range of 10%–15% were quite frequently occurring (figures 8–12). It can also be observed that the differences between the average and convolved dose distributions were much smaller, and hence the dosimetric effects of interplay average out for multiple fractions. Further, large differences were observed between the simulated dose distributions for the different initial breathing phases, implying a large impact of the initial breathing phase on the interplay effects.

The dosimetric effects of interplay varied considerably with the different patient- and machine specific parameters investigated, and the following trends were observed:

- The $\Delta D_{98\%}$ and $\Delta D_{2\%}$ decreased and increased, respectively, for longer period times (figure 8).
- Lower $\Delta D_{98\%}$ and higher $\Delta D_{2\%}$ were observed for increasing breathing amplitudes up to approximately 20 mm, after which small increases in $\Delta D_{98\%}$ and decreases in $\Delta D_{2\%}$ were observed (figure 8).
- Lower $\Delta D_{98\%}$ and higher $\Delta D_{2\%}$ was observed for increased number of MU/Gy (figure 9), indicating a larger dosimetric effect of interplay for more complex treatment plans.
- The $\Delta D_{98\%}$ and $\Delta D_{2\%}$ decreased and increased, respectively, for lower dose levels (figure 10).
- The $\Delta D_{98\%}$ were lower and $\Delta D_{2\%}$ higher for FFF compared to FF (figure 10).
- The magnitude of $\Delta D_{98\%}$ and $\Delta D_{2\%}$ did not differ much for the different CTV sizes (figure 11). However, a larger spread in $\Delta D_{98\%}$ and $\Delta D_{2\%}$ between the different initial breathing phases were observed for the smaller CTV sizes (Ø 1 and 3 cm), indicating that the initial breathing phase has a larger impact of the interplay effects for smaller CTV volumes.
- Only small differences in $\Delta D_{98\%}$ and $\Delta D_{2\%}$ were observed for the different collimator angles (figure 12), although slightly larger values can be seen for 30 and 45° compared to 0 and 90°.
- Both $\Delta D_{98\%}$ and $\Delta D_{2\%}$ varies considerably with the initial breathing phase (figures 8–12).
- Much higher $\Delta D_{98\%}$ and lower $\Delta D_{2\%}$ were observed for the average dose distribution, representing multiple fractions (figures 8–12).

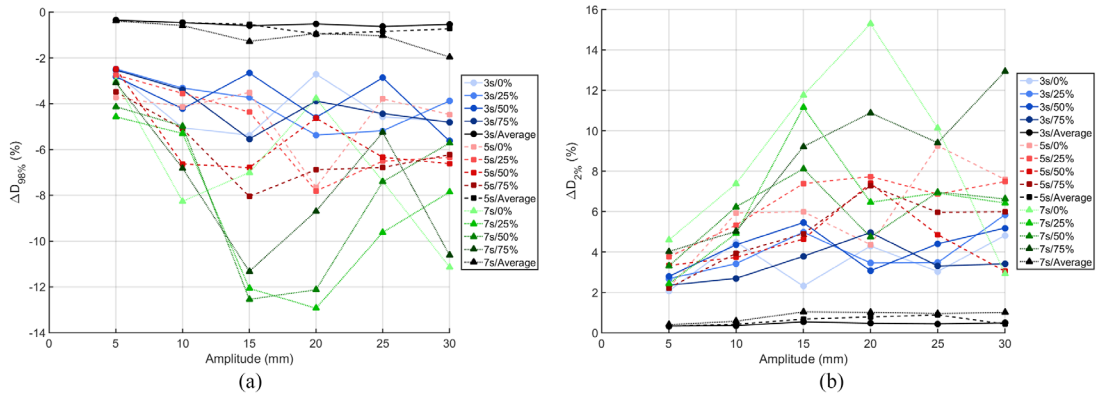

Figure 8. The $\Delta D_{98\%}$ (a) and $\Delta D_{2\%}$ (b) of the difference between the simulated and convolved dose distributions as a function of the breathing amplitude for the period times 3 s (blue circles, solid lines), 5 s (red squares, dashed lines) and 7 s (green triangles, dotted lines), with the different initial breathing phases (0, 25, 50 and 75%) displayed in different color shades. Also, the $\Delta D_{98\%}$ and $\Delta D_{2\%}$ for the difference between the average dose distribution of the four initial breathing phases and the convolved dose distribution are displayed in black, representing the effect of multiple fractions. The lines are for illustration purpose only.

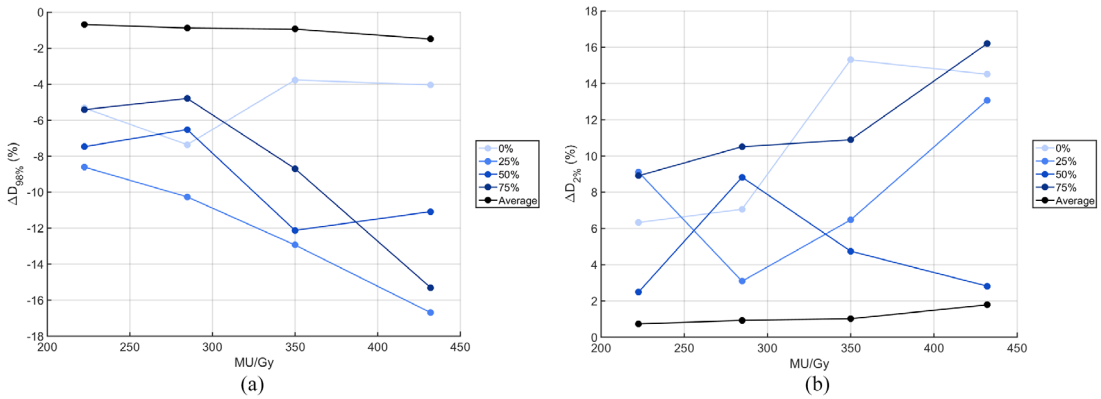

Figure 9. The $\Delta D_{98\%}$ (a) and $\Delta D_{2\%}$ (b) of the difference between the simulated and convolved dose distributions as a function of number of MU/Gy (different plan complexities), with the different initial breathing phases (0, 25, 50 and 75%) displayed in different shades of blue. Also, the $\Delta D_{98\%}$ and $\Delta D_{2\%}$ for the difference between the average dose distribution of the four initial breathing phases and the convolved dose distribution are displayed in black, representing the effect of multiple fractions. The lines are for illustration purpose only.

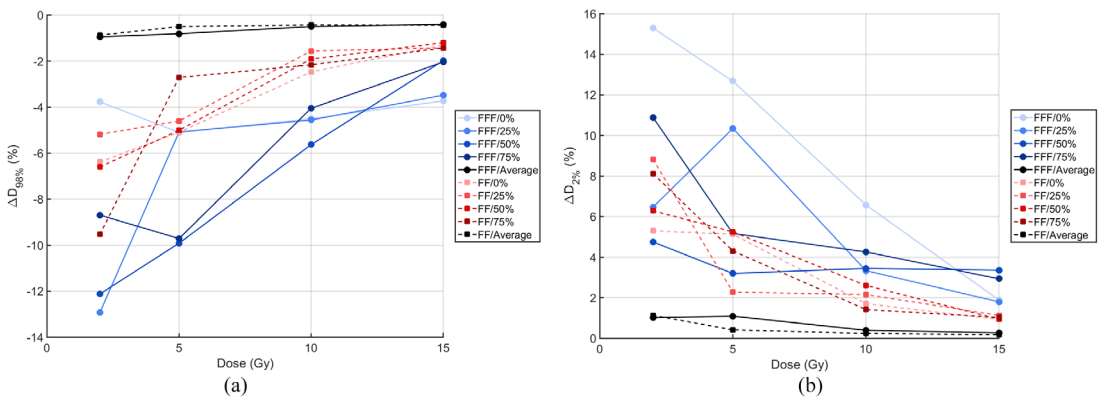

Figure 10. The $\Delta D_{98\%}$ (a) and $\Delta D_{2\%}$ (b) of the difference between the simulated and convolved dose distributions as a function of dose level for FFF (blue circles, solid lines) and FF (red squares, dashed lines), with the different initial breathing phases (0, 25, 50 and 75%) displayed in different color shades. Also, the $\Delta D_{98\%}$ and $\Delta D_{2\%}$ for the difference between the average dose distribution of the four initial breathing phases and the convolved dose distribution are displayed in black, representing the effect of multiple fractions. The lines are for illustration purpose only.

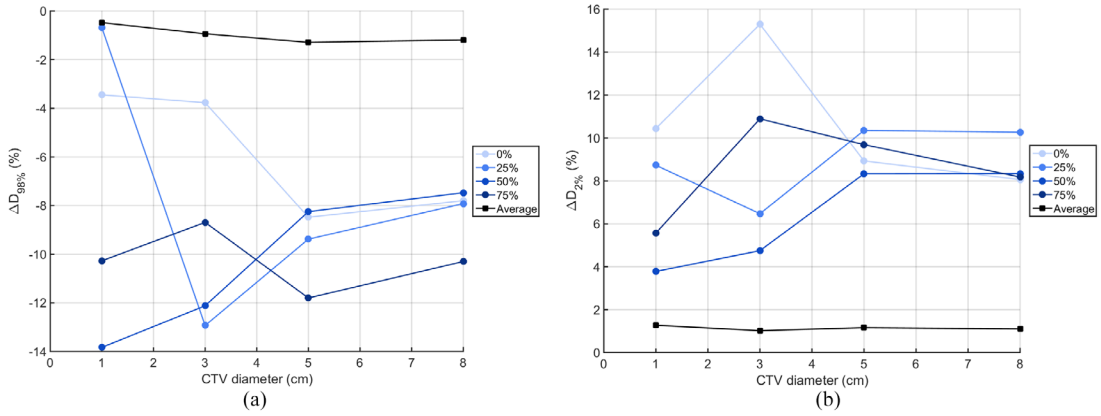

Figure 11. The $\Delta D_{98\%}$ (a) and $\Delta D_{2\%}$ (b) of the difference between the simulated and convolved dose distributions as a function of CTV diameter with the different initial breathing phases (0, 25, 50 and 75%) displayed in different shades of blue. Also, the $\Delta D_{98\%}$ and $\Delta D_{2\%}$ for the difference between the average dose distribution of the four initial breathing phases and the convolved dose distribution are displayed in black, representing the effect of multiple fractions. The lines are for illustration purpose only.

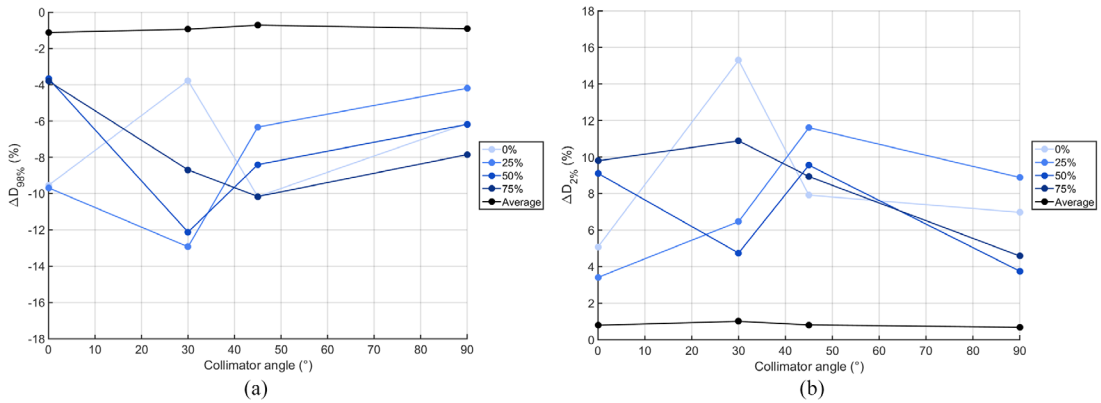

Figure 12. The $\Delta D_{98\%}$ (a) and $\Delta D_{2\%}$ (b) of the difference between the simulated and convolved dose distributions as a function of collimator angle, with the different initial breathing phases (0, 25, 50 and 75%) displayed in different shades of blue. Also, the $\Delta D_{98\%}$ and $\Delta D_{2\%}$ for the difference between the average dose distribution of the four initial breathing phases and the convolved dose distribution are displayed in black, representing the effect of multiple fractions. The lines are for illustration purpose only.

4. Discussion

In this study, a simulation tool using a commercial TPS was developed to quantify the dosimetric effects of motion induced interplay for RapidArc treatment. In addition, the simulation tool was verified by comparison with dosimetric measurements. Extensive interplay effects were observed for individual fractions, resulting in both over- and under-dosed volumes of the CTV. A large number of treatment scenarios were simulated, and the extent of interplay effects varied largely with the different patient- and machine specific parameters investigated.

4.1. The simulation tool

The developed simulation tool has many applications and is available upon request. It could be used to estimate the dosimetric effect of interplay for individual patient treatments, which would give an indication of the extent of interplay effects that could be expected for that specific patient treatment. This kind of tool could also be useful on a population basis to develop more general guidelines for RapidArc treatments of moving tumours. For instance, it could be used to determine which combination of patient- and machine specific parameters that could be allowed to keep the dosimetric effect of interplay below a certain tolerance level, for example to keep $\Delta D_{98\%}$ and $\Delta D_{2\%}$ less than $\pm 10\%$.

Since interplay effects were separated from dose blurring, all results presented in this study includes only the effect of interplay. This was achieved through (1) the creation of an ITV in the treatment planning process to avoid the dose blurring effects at the edge of the target and (2) by convolving the original dose distribution with the motion pattern to remove the dose blurring in the central parts of the CTV. The edge effect was by far the dominating of these two effects and only very small differences were observed when subtracting the simulated and convolved dose distributions, compared to subtracting the simulated and original dose distributions. This is

probably due to the relatively homogeneous dose distribution within the CTV in the original (static) treatment plans.

A $\sin^6$ motion pattern was used in this study, since it has previously been shown to be more representative of patient breathing than a sin motion pattern (Seppenwoolde *et al* 2002). Also, Seco *et al* (2007) compared sin, $\sin^4$ and $\sin^6$ for IMRT, and showed largest dosimetric effects of interplay for $\sin^6$ motion. However, the use of $\sin^6$ implies a perfect cyclic respiration, which is not completely representative of real patient breathing, which tend to be much more irregular with changing amplitude and period time, as well as baseline drifts (Seppenwoolde *et al* 2002). In our simulation method, any motion pattern could be implemented, which would allow interplay effects for real patient respiratory motion to be investigated in the future.

Many previous studies investigating motion induced interplay effects are based on measurements, which is a rather time consuming process. One major advantage of the method developed in this study is that it is based on simulations in a commercial TPS using an advanced dose calculation algorithm (AAA). Hence, it is much faster compared to measurements, and thereby allows for a large number of different treatment scenarios to be investigated. In total, 136 different combinations of patient- and machine specific parameters were simulated in this study. However, it was still not possible to simulate all possible combinations of the parameters, since the dose calculation was still rather time consuming due to the large amount of sub-arcs in some of the treatment plans. The low spatial resolution of the position bins of 1 mm resulted in an average number of sub-arcs of 573 with a range of 82–2664. Hence, other parameter combinations may exist that would result in even larger interplay effects than those presented here. Another limitation of the present simulation method is that only rigid motion is included and that deformations as well as changes in radiological path length are not accounted for. Also, the simulation method developed is only valid for the Eclipse TPS, and hence the results presented in this study are representative only for this TPS. The extent of interplay effects for other TPSs may be different, since their optimizers work differently. For instance, other MLC sequences are generated, which may be more or less complex, and hence it would be interesting to compare the extent of interplay effects generated by different TPSs. Despite these limitations, we believe this simulation method gives a good indication of the extent of interplay effects to be expected for the various treatment scenarios investigated.

4.2. Verification measurements

Regarding the verification measurements, good agreement was observed between the simulated and measured dose distributions including motion. Even slightly higher gamma pass rates were observed compared to the static measurements and original dose distributions not including effects of motion, which is probably because the motion dose distributions are blurred and hence have less steep dose gradients compared to the static dose distributions. The relatively low gamma pass rates around 93% for some of the measurements are probably due to the high complexity of these plans. For the measured plan with the lowest complexity level (C_1), the gamma pass rate was 100% for the criteria 3%/2 mm global dose. Hence, the proposed simulation method was verified and could thus be used for further simulations to investigate how interplay effects depend on different patient- and machine specific parameters.

4.3. Dependence on patient- and machine specific parameters

Although trends of the dependence of the dosimetric effect of interplay on the different parameters investigated can be observed in figures 8–12, these are not always very explicit. This is because the interference of particular combinations of breathing patterns and machine-related parameters may give rise to large interplay effects. This is also the reason for the large variation in the dosimetric effects of interplay observed between the different initial breathing phases (figures 5–12). For example, if the beam is turned on in two different breathing phases this cause completely different mutual movement between the target and the MLC, resulting in different extent of interplay effects. This makes the extent of interplay effects for a real patient treatment extremely hard to predict, since the initial breathing phase of the treatment delivery is usually not known.

4.3.1. Breathing pattern

In figure 8, it can be seen that the dosimetric effect of interplay generally increased for larger breathing amplitudes and longer period times, with some exceptions for breathing amplitudes larger than 20 mm. This is consistent with previous studies, showing increased interplay effects for larger tumour motion and longer period times (Court *et al* 2008, 2010, Ong *et al* 2011, 2013). The dose deviations due to interplay effects will to a greater extent average out if several respiratory cycles pass while the plan is delivered. This is the reason for the increased dosimetric effect of interplay observed for longer period times since, for a delivery time of 1 min, the number of full respiratory cycles are 19, 11 and 8 for the period times 3, 5 and 7 s, respectively.

4.3.2. Plan complexity

The dosimetric effects of interplay generally increased for higher number of MU/Gy, i.e. for more complex treatment plans (figure 9), which has also been shown in previous studies (Court *et al* 2010, Ong *et al* 2011). It should be mentioned that the number of MU/Gy may not be a perfect measure of the plan complexity (i.e. more MLC movement and smaller field openings), since it would be possible to increase the number of MU/Gy for a treatment plan without actually increasing the complexity, and more advanced complexity metrics could be used (Gotstedt *et al* 2015). However, reviewing the treatment plans in this study, it appears as if the complexity of all plans increased for higher number of MU/Gy.

4.3.3. Dose level and FF/FFF

Longer delivery times implies that more respiratory cycles will pass during the treatment delivery. This explains why the dosimetric effect of interplay increases for FFF (higher dose rate) compared to FF and for lower dose levels (figure 10), since the delivery time will then be shorter (table 1). For example, the treatment times were 1.00, 1.06, 2.50 and 5.16 min for 2 Gy FFF, 2 Gy FF, 10 Gy FFF and 10 Gy FF, respectively, corresponding to 8–19, 9–21, 21–50 and 44–103 full respiratory cycles, depending on the period time. Another possible reason that the interplay effects are higher for FFF plans and lower dose levels (shorter delivery times) could be that the MLC speed is higher for these plans, which could result in more complex MLC sequences. These results are in accordance with previous studies, where Ong *et al* (2013) showed increased interplay effects for FFF compared to FF stereotactic lung radiotherapy using VMAT. Moreover, Court *et al* (2008) and Jiang *et al* (2003) showed increased interplay effects for higher dose rates for IMRT. Also, Rao *et al* (2012) showed increased interplay effects for a single conventional fraction of 2 Gy compared to a single stereotactic fraction of 20 Gy, for both VMAT and IMRT lung radiotherapy.

4.3.4. CTV size

The magnitude of the dosimetric effect of interplay did not vary much between different CTV sizes (figure 11). For smaller CTV sizes, however, the initial breathing phase has a larger impact on the interplay effects. The size of the hot- and cold spots in the simulated dose distributions (figure 6) is approximately the same irrespective of the CTV size, as the width of the MLC is the same. Since the volumes of the smaller CTVs investigated (Ø 1 and 3 cm) are in the same order of magnitude as the volumes of the hot- and cold spots generated in the simulated dose distributions, the CTV volume could be completely dominated by either a hot spot or a cold spot. This makes the dosimetric effect of interplay more dependent on the initial breathing phase for smaller CTV sizes, which appears as a large spread in $\Delta D_{98\%}$ and $\Delta D_{2\%}$ for the different initial breathing phases in figure 11.

4.3.5. Collimator angle

Different collimator angles were simulated to investigate if interplay effects depend on the relative direction between the breathing motion and the motion of the MLC, where the collimator angles 0 and 90° correspond to the breathing motion and MLC motion being perpendicular and parallel, respectively. Only small differences were observed between the different collimator angles, although slightly larger interplay effects were observed for 30° and 45° compared to 0° and 90° (figure 12). The collimator angles 30° and 45° are commonly used clinically, whereas 0° and 90° are not, to minimize the tongue-and-groove effect and interleaf leakage (Deng *et al* 2001). Court *et al* (2008) showed larger interplay effects for parallel motion compared to perpendicular motion for sliding window IMRT, which was not observed in this study for RapidArc treatment.

4.4. Multiple fractions

In this study, we have shown that motion induced interplay effects for RapidArc treatment result in heterogeneous dose distributions for individual treatment fractions. However, these dosimetric heterogeneities were substantially reduced for multiple fractions due to averaging effects, which has also been shown in previous studies (Bortfeld *et al* 2002, 2004, Jiang *et al* 2003, Duan *et al* 2006, Court *et al* 2010, Rao *et al* 2012, Ong *et al* 2013). However, since it is not known whether or not this averaging also applies to the biological effect, we would like to highlight the importance of investigating the dosimetric effect of interplay for individual fractions and not only for the accumulated dose of the whole treatment. Also, this averaging effect only applies for an even distribution of initial breathing phases, which is more probable for an increasing number of fractions. For a low number of fractions, which is used in hypofractionated treatment, the probability of starting the treatment in the same phase for each fraction is larger, and hence the averaging effects would be less pronounced.

4.5. Mitigation of interplay effects

According to this study, the dosimetric effects of interplay could be mitigated by reducing the complexity of the treatment plan and/or lowering the dose-rate (i.e. to use FF instead of FFF). However, lowering the dose-rate

leads to prolonged treatment times, increasing the likelihood of patient motion during the treatment delivery. Also, special care should be taken before using VMAT treatment for patients experiencing target motions with large amplitude and long period time. Other methods presented in the literature shown to mitigate interplay effects are the use of respiratory gating in combination with VMAT (Nicolini *et al* 2010, Qian *et al* 2011, Riley *et al* 2014, Viel *et al* 2015), tracking (Ceberg *et al* 2010, Keall *et al* 2014), and the use of conformal arcs (Dickey *et al* 2015).

Hypofractionation, where the treatment is given in few high dose fractions, is increasingly used and it has been proposed that interplay might be a greater concern for this type of treatment since the averaging effect from multiple fractions is reduced (Ong *et al* 2011, 2013, Rao *et al* 2012). However, larger dose per fraction is then given, resulting in lower interplay effects according to this study (figure 10). Also, FFF may be used to reduce the treatment time for hypofractionated treatments, which again results in larger interplay effects. Interplay effects for hypofractionated FFF VMAT treatment require further work. We therefore plan to continue our investigation to study the dosimetric effects of interplay for hypofractionated FFF VMAT treatment of liver tumours, by applying the developed simulation method on four-dimensional (4D) computed tomography images of real patients, and to use deformable image registration to calculate the dynamically accumulated dose in 4D.

5. Conclusions

A tool to simulate motion induced interplay effects for RapidArc treatment was developed and verified with measurements, which allowed interplay effects for a large number of treatment scenarios to be investigated. Large interplay effects were observed for individual fractions and the extent varied with the patient- and machine specific parameters investigated. Generally, interplay effects were larger for FFF compared to FF and increased for higher breathing amplitudes, longer period times, lower dose levels and more complex treatment plans. Also, the interplay effects varied considerably with the initial breathing phase and larger variations were observed for smaller CTV sizes.

References

Bortfeld T, Jiang S B and Rietzel E 2004 Effects of motion on the total dose distribution *Semin. Radiat. Oncol.* **14** 41–51

Bortfeld T, Jokivarsi K, Goitein M, Kung J and Jiang S B 2002 Effects of intra-fraction motion on IMRT dose delivery: statistical analysis and simulation *Phys. Med. Biol.* **47** 2203–20

Ceberg S, Ceberg C, Falk M, af Rosenschöld P M and Bäck S Å J 2013 Evaluation of breathing interplay effects during VMAT by using 3D gel measurements *J. Phys.: Conf. Ser.* **444** 012098

Ceberg S *et al* 2010 Tumor-tracking radiotherapy of moving targets; verification using 3D polymer gel, 2D ion-chamber array and biplanar diode array *J. Phys.: Conf. Ser.* **250** 012051

Court L, Wagar M, Berbeco R, Reisner A, Winey B, Schofield D, Ionascu D, Allen A M, Popple R and Lingos T 2010 Evaluation of the interplay effect when using RapidArc to treat targets moving in the craniocaudal or right–left direction *Med. Phys.* **37** 4–11

Court L, Wagar M, Ionascu D, Berbeco R and Chin L 2008 Management of the interplay effect when using dynamic MLC sequences to treat moving targets *Med. Phys.* **35** 1926–31

Deng J, Pawlicki T, Chen Y, Li J, Jiang S B and Ma C M 2001 The MLC tongue-and-groove effect on IMRT dose distributions *Phys. Med. Biol.* **46** 1039–60

Dickey M, Roa W, Drodge S, Ghosh S, Murray B, Scrimger R and Gabos Z 2015 A planning comparison of 3-dimensional conformal multiple static field, conformal arc, and volumetric modulated arc therapy for the delivery of stereotactic body radiotherapy for early stage lung cancer *Med. Dosim.* **40** 347–51

Duan J, Shen S, Fiveash J B, Popple R A and Brezovich I A 2006 Dosimetric and radiobiological impact of dose fractionation on respiratory motion induced IMRT delivery errors: a volumetric dose measurement study *Med. Phys.* **33** 1380–7

Gotstedt J, Karlsson Hauer A and Back A 2015 Development and evaluation of aperture-based complexity metrics using film and EPID measurements of static MLC openings *Med. Phys.* **42** 3911–21

Jagsi R, Falchook A D, Hendrix L H, Curry H and Chen R C 2014 Adoption of hypofractionated radiation therapy for breast cancer after publication of randomized trials *Int. J. Radiat. Oncol. Biol. Phys.* **90** 1001–9

Jiang S B, Pope C, Al Jarrah K M, Kung J H, Bortfeld T and Chen G T 2003 An experimental investigation on intra-fractional organ motion effects in lung IMRT treatments *Phys. Med. Biol.* **48** 1773–84

Keall P J, Colvill E, O'Brien R, Ng J A, Poulsen P R, Eade T, Kneebone A and Booth J T 2014 The first clinical implementation of electromagnetic transponder-guided MLC tracking *Med. Phys.* **41** 020702

Low D A, Harms W B, Mutic S and Purdy J A 1998 A technique for the quantitative evaluation of dose distributions *Med. Phys.* **25** 656–61

Lujan A E, Larsen E W, Balter J M and Ten Haken R K 1999 A method for incorporating organ motion due to breathing into 3D dose calculations *Med. Phys.* **26** 715–20

Nicolini G, Vanetti E, Clivio A, Fogliata A and Cozzi L 2010 Pre-clinical evaluation of respiratory-gated delivery of volumetric modulated arc therapy with RapidArc *Phys. Med. Biol.* **55** 347–57

Nordström F 2012 Quality assurance in radiotherapy—development and evaluation of new tools for improved patient safety *PhD Thesis*, Lund University (http://lup.lub.lu.se/record/2493127)

Nordström F, Af Wetterstedt S and Bäck S Å J 2013 4D dosimetry and its applications to pre-treatment quality control and real-time *in vivo* dosimetry of VMAT treatments *J. Phys.: Conf. Ser.* **444** 012021

Nyholm T, Berglund M, Brynolfsson P and Jonsson J 2015 EP-1533: ICE-studio—an interactive visual research tool for image analysis *Radiother. Oncol.* **115** S837

Ong C L, Dahele M, Slotman B J and Verbakel W F 2013 Dosimetric impact of the interplay effect during stereotactic lung radiation therapy delivery using flattening filter-free beams and volumetric modulated arc therapy *Int. J. Radiat. Oncol. Biol. Phys.* **86** 743–8

Ong C L, Verbakel W F, Cuijpers J P, Slotman B J and Senan S 2011 Dosimetric impact of interplay effect on RapidArc lung stereotactic treatment delivery *Int. J. Radiat. Oncol. Biol. Phys.* **79** 305–11

Otto K 2008 Volumetric modulated arc therapy: IMRT in a single gantry arc *Med. Phys.* **35** 310–7

Park J M, Park S Y, Kim H, Kim J H, Carlson J and Ye S J 2014 Modulation indices for volumetric modulated arc therapy *Phys. Med. Biol.* **59** 7315–40

Poulsen P R, Schmidt M L, Keall P J, Worm E S, Fledelius W and Hoffmann L 2012 A method of dose reconstruction for moving targets compatible with dynamic treatments *Med. Phys.* **39** 6237–46

Qian J, Xing L, Liu W and Luxton G 2011 Dose verification for respiratory-gated volumetric modulated arc therapy *Phys. Med. Biol.* **56** 4827–38

Rao M, Wu J, Cao D, Wong T, Mehta V, Shepard D and Ye J 2012 Dosimetric impact of breathing motion in lung stereotactic body radiotherapy treatment using intensity modulated radiotherapy and volumetric modulated arc therapy *Int. J. Radiat. Oncol. Biol. Phys.* **83** 251–6

Riley C, Yang Y, Li T, Zhang Y, Heron D E and Huq M S 2014 Dosimetric evaluation of the interplay effect in respiratoty-gated RapidArc radiation therapy *Med. Phys.* **41** 011715

Seco J, Sharp G C, Turcotte J C, Gierga D P, Bortfeld T and Paganetti H 2007 Effects of organ motion on IMRT treatments with segments of few monitor units *Med. Phys.* **34** 923–34

Seppenwoolde Y, Shirato H, Kitamura K, Shimizu S, Van Herk M B, Lebesque J V and Miyasaka K 2002 Precise and real-time measurements of 3D tumor motion in lung due to breathing and heartbeat, measured during radiotherapy *Int. J. Radiat. Oncol. Biol. Phys.* **53** 822–34

Stokes W A, Kavanagh B D, Raben D and Pugh T J 2017 Implementation of hypofractionated prostate radiation therapy in the United States: A National Cancer Database analysis *Pract. Radiat. Oncol.* **7** 270–8

Viel F, Lee R, Gete E and Duzenli C 2015 Amplitude gating for a coached breathing approach in respiratory gated 10 MV flattening filter-free VMAT delivery *J. Appl. Clin. Med. Phys.* **16** 79–90